Journal of the Operations Research
Society of Japan
Vol. 39, No. 4, December 1996

TAIL BEHAVIOR OF THE STEADY-STATE DISTRIBUTION IN TWO-STAGE TANDEM QUEUES: NUMERICAL EXPERIMENT AND CONJECTURE

Kou Fujimoto Yukio Takahashi
Tokyo Institute of Technology

(Received January 10, 1995; Final February 15, 1996)

Abstract This paper is concerned with the geometric decay property of the steady-state probability $x(n_1, n_2; i_0, i_1, i_2)$ in a tandem queueing system $PH/PH/1 \rightarrow /PH/1$. First we observe results of an extensive numerical experiment and see two types of geometric decay for the tail of the joint queue-length distribution depending on the traffic intensities of the first and second stages. Then, based on the observation, we give a conjecture on the geometric decay property. The conjecture is roughly summarized as follows.

For a given traffic intensity ρ_1 of the first stage, there exists a threshold $\tilde{\rho}_2$ for the traffic intensity ρ_2 of the second stage, and if $\rho_2 < \tilde{\rho}_2$, then the joint queue-length probability $p(n_1, n_2) \sim G\eta_1^{n_1}\eta_2^{n_2}$ as $n_1, n_2 \rightarrow \infty$. If $\rho_2 > \tilde{\rho}_2$, then $p(n_1, n_2)$ decays in a similar manner, but the coefficient G and the decay rates η_1, η_2 are different between the cases with $n_2 < \tilde{a}n_1$ and with $n_2 > \tilde{a}n_1$ for a certain positive value $\tilde{a}$. Moreover, the conditional probability of phases $y(i_0, i_1, i_2 \mid n_1, n_2) = x(n_1, n_2; i_0, i_1, i_2)/p(n_1, n_2)$ is asymptotically independent of n_1 and n_2 in each case, and hence the steady-state distribution has geometric tail. Equations are also given for determining characteristic values $\tilde{\rho}_2, \eta_1, \eta_2$ and $\tilde{a}$.

1. Introduction

Tandem queueing systems are basic models in the queueing theory and have been studied for a long time. However, the stationary state probabilities, or even basic properties of them, are scarcely known except for some simple cases with product form solutions. In this paper, we observe the tail behavior of the stationary joint queue-length distribution in a two-stage tandem queueing system $PH/PH/1 \rightarrow /PH/1$ with buffers of infinite capacity.

In the ordinary one-stage queue $PH/PH/c$ with traffic intensity $\rho < 1$, it is shown that the steady-state distribution has a geometric tail [2, 5]. Namely, if we let $x(n; i_0, i_1)$ be the steady-state probability that there are n customers in the system while the states (phases) of arrival and service processes are i_0 and i_1, then

$$x(n; i_0, i_1) \sim Gc_0(i_0)c_1(i_1)\eta^n, \quad n \rightarrow \infty, \tag{1.1}$$

where $\eta, G, c_0(i_0)$ and $c_1(i_1)$ are constants, and hence

$$\frac{x(n+1; i_0, i_1)}{x(n; i_0, i_1)} \sim \eta, \quad n \rightarrow \infty, \tag{1.2}$$

where $\sim$ indicates that the ratio of both sides tends to 1.

The decay rate η is given in the following manner. Let $T^*(s)$ and $S^*(s)$ be the Laplace-Stieltjes transforms (LSTs) of the interarrival and service time distributions, respectively, and let ω be the unique positive solution of the equation $T^*(s)S^*(-cs) = 1$. Then $\eta = T^*(\omega)$.

This geometric decay property is very useful, for example, on the computation of the stationary state probabilities and on the discussion of tail probabilities for estimating very small loss probabilities (e.g. less than 10^{-9}) of the corresponding finite queue.

The problem here is to see whether a similar geometric tail property holds or not in two-stage tandem queueing systems.

The marginal queue-length distribution of the first stage clearly has a geometric tail, since the behavior of the first stage is not affected by that of the second stage. Our concern is the tail property of the joint queue-length distribution of the first and second stages or the state probabilities in the steady state.

To see it, we make an extensive numerical experiment though the types of models are limited to simple ones because of the limitation of the sizes of computable models. We scrutinize the results and find two types of geometric decay depending on the traffic intensities of the first and second stages. To the authors' knowledge, this fact has never reported so far in the literature. Based on the observations of the numerical results, we give a conjecture on the geometric decay together with systems of equations which determine the parameters in the conjecture. The authors think that the property stated in the conjecture will not only be useful for practical computation or simulation of two stage tandem queueing systems, but also will provide a key to further theoretical researches for tandem queueing systems.

This paper is organized as follows. In Section 2, we describe our tandem queueing model and present our conjecture on geometric tail of the steady-state distribution. In Section 3, we explain our numerical experiment briefly. Section 4 presents various numerical results which show the tail properties we conjecture in Section 2. We discuss, in Section 5, some equations which determine parameters used in the conjecture.

2. The Model and the Conjecture

Here we introduce our two-stage tandem queueing model and give a conjecture on the geometric tail. We also show some numerical results which support the conjecture in a variety of cases.

We denote by $PH(\boldsymbol{a}, \boldsymbol{Q})$ a phase-type distribution with initial probability vector $\boldsymbol{a}$ and infinitesimal generator $\boldsymbol{Q}$.

2.1. Two-stage Tandem Queueing System $PH/PH/1 \rightarrow /PH/1$

We consider an open, two-stage tandem queueing system (Figure 1). Customers arrive at the first stage to be served there, move to the second to be served there again, and then go out of the system. The queueing discipline is the ordinary first-in-first-out (FIFO). The kth stage ($k = 1, 2$) has a single server and a buffer of infinite capacity, so that no loss or blocking occurs. Interarrival times of customers are independent and identically distributed (i.i.d.) random variables subjecting to a phase-type distribution $PH(\boldsymbol{\alpha}, \boldsymbol{T})$. Service times at the kth stage are also i.i.d. variables subjecting to a phase-type distribution $PH(\boldsymbol{\beta}_k, \boldsymbol{S}_k)$. The interarrival and service times are assumed to be mutually independent.

The state of the system is represented by a quintuple $(n_1, n_2; i_0, i_1, i_2)$, where i_0 is the phase of the arrival process, i_k is the phase of the service process at the kth stage, and n_k is the number of customers in the kth stage ($k = 1, 2$). Then the system behaves as a time-continuous Markov chain.

We denote the traffic intensity at the kth stage by $\rho_k = \lambda/\mu_k$ where $1/\lambda$ is the mean interarrival time and $1/\mu_k$ is the mean service time at the kth stage ($k = 1, 2$). We assume $\rho_1, \rho_2 < 1$ so that the chain is stable and has steady-state probabilities $x(n_1, n_2; i_0, i_1, i_2)$.

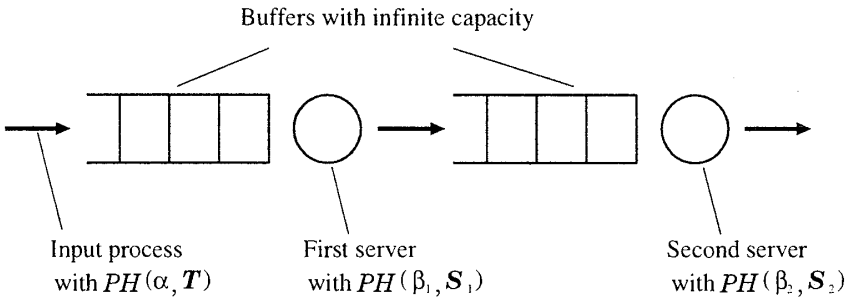

Figure 1: Two-stage tandem queues

2.2. Geometric Decay Property from the Numerical Experiment and the Conjecture

The tail property extracted from the numerical results is roughly summarized as follows.

For a given traffic intensity ρ_1 of the first stage, there exists a threshold $\tilde{\rho}_2$ for the traffic intensity ρ_2 of the second stage, and if $\rho_2 < \tilde{\rho}_2$, then the joint queue-length probability $p(n_1, n_2)$ is asymptotically of the geometric form

$$p(n_1, n_2) \sim G\ \eta_1^{n_1}\eta_2^{n_2} \quad (n_1, n_2 \to \infty). \tag{2.1}$$

If $\rho_2 > \tilde{\rho}_2$, then $p(n_1, n_2)$ decays in a similar manner, but the coefficient G and the decay rates η_1, η_2 are different between the cases with $n_2 < \tilde{a}n_1$ and with $n_2 > \tilde{a}n_1$ for a certain positive value $\tilde{a}$. Moreover, the conditional probability of phases $y(i_0, i_1, i_2 \mid n_1, n_2) = x(n_1, n_2; i_0, i_1, i_2)/p(n_1, n_2)$ is asymptotically independent of n_1 and n_2 in each case, and hence the steady-state distribution has geometric tail.

To describe the geometric decay property more formally, however, we should clarify the way of making n_1 and n_2 large in (2.1). Here we consider the case in which n_1 and n_2 increase on a line $n_2 = an_1 + b$. To ensure that there exist infinitely many points (n_1, n_2) on the line, the coefficient a should be positive and rational and the constant b rational. As extreme cases, we also consider the case in which $n_1 \to \infty$ with fixed n_2 and the case in which $n_2 \to \infty$ with fixed n_1.

The conjecture we make in this paper is formally stated as follows.

Conjecture

For fixed ρ_1, there exists a threshold $\tilde{\rho}_2$ and the behavior of $x(n_1, n_2; i_0, i_1, i_2)$ is different between the cases $\rho_2 < \tilde{\rho}_2$ and $\rho_2 > \tilde{\rho}_2$.

1. In the case $\rho_2 < \tilde{\rho}_2$, there exist constants $\eta_1, \eta_2, c_0(i_0), c_1(i_1), c_2(i_2)$ and G such that

$$x(n_1, n_2; i_0, i_1, i_2) \sim G\ c_0(i_0)c_1(i_1)c_2(i_2)\eta_1^{n_1}\eta_2^{n_2}$$

as $n_1, n_2 \to \infty$ on a line $n_2 = an_1 + b$ with rational $a > 0$ and b. This asymptotic representation is also valid when $n_1 \to \infty$ with fixed n_2 and when $n_2 \to \infty$ with fixed n_1.

2. In the case $\rho_2 > \tilde{\rho}_2$, there exists a positive constant $\tilde{a}$ such that the decay rates are different between the cases $0 < a < \tilde{a}$ and $a > \tilde{a}$ for the slope a of the line on which n_1 and n_2 increase. We denote the two sets of constants corresponding to these two cases as $\{\eta_1, \eta_2, c_0(i_0), c_1(i_1), c_2(i_2), G\}$ and $\{\overline{\eta}_1, \overline{\eta}_2, \overline{c}_0(i_0), \overline{c}_1(i_1), \overline{c}_2(i_2), \overline{G}\}$.

(a) When $n_1, n_2 \to \infty$ on a line $n_2 = an_1 + b$ with rational a and b such that $0 < a < \tilde{a}$,

$$x(n_1, n_2; i_0, i_1, i_2) \sim G\ c_0(i_0)c_1(i_1)c_2(i_2)\eta_1^{n_1}\eta_2^{n_2}.$$

This asymptotic representation is also valid when $n_1 \to \infty$ with fixed n_2.

(b) When $n_1, n_2 \to \infty$ on a line $n_2 = an_1 + b$ with rational a and b such that $a > \tilde{a}$,

$$x(n_1, n_2; i_0, i_1, i_2) \sim \overline{G}\ \overline{c}_0(i_0)\overline{c}_1(i_1)\overline{c}_2(i_2)\overline{\eta}_1^{n_1}\overline{\eta}_2^{n_2}.$$

This asymptotic representation is also valid when $n_2 \to \infty$ with fixed n_1.

3. The constants above are determined by equations given in the latter sections as indicated by the equation numbers:

η_1, η_2 .....(5.3)
$\overline{\eta}_1, \overline{\eta}_2$ ..... (5.5)
$\tilde{\rho}_2$ .....(5.6)
$\tilde{a}$ ..... (4.4), (5.7)
$c_k(i_k), \overline{c}_k(i_k)$ $(k = 0, 1, 2)$ ...(5.8)

Unfortunately we do not yet have any equations to determine the values of the multiplicative coefficients G and $\overline{G}$. On the point, see comments at the end of Section 5.

2.3. Numerical Test for the Conjecture

To see if the asymptotic property stated in the conjecture above holds or not, we tabulate the values of the ratios

$$g(n_1, n_2) = \frac{p(n_1, n_2)}{\eta_1^{n_1}\eta_2^{n_2}} \quad \text{and} \quad \overline{g}(n_1, n_2) = \frac{p(n_1, n_2)}{\overline{\eta}_1^{n_1}\overline{\eta}_2^{n_2}}.$$

in Tables 1 and 2 for eight types of models with selected pair of traffic intensities (ρ_1, ρ_2) and selected points (n_1, n_2) lying on lines $n_2 = 4n_1 - 5$ and $n_2 = (n_1 + 5)/4$. All these values are extracted from the results of a numerical experiment described in Section 3.

These tables show that each row certainly converges to a positive limit, even though the speed of convergence is much slower in a few cases (see Table 2(b)). In Table 1, the ratios along two different lines seem to converge to a common limit in each model. This corresponds to the first statement of the conjecture. In Table 2, these ratios seem to converge to different limits in each model. This agrees with the second statement of the conjecture. These numerical results support the geometric tail property of the joint queue-length distribution. The asymptotic independence of phases is shown in Tables 4 and 5 in Section 4.3 for a particular model $E_2/H_2/1 \to /E_2/1$ with $\rho_1 = 0.6$ and $\rho_2 = 0.8$.

The authors tested the conjecture for more than 1,000 cases. There are a small number of cases in which the convergence of $g(n_1, n_2)$ and/or $\overline{g}(n_1, n_2)$ cannot be judged from the numerical results of $p(n_1, n_2)$ with $n_1, n_2 \leq 100$. The authors think that, if we can calculate $p(n_1, n_2)$ for larger n_1 and n_2, we will be able to see the convergence numerically. Except these slow converging cases, $g(n_1, n_2)$ and $\overline{g}(n_1, n_2)$ do converge numerically to certain limits in all the cases we tested.

3. Numerical Experiment

To see the tail behavior of the joint queue-length distribution, we made an extensive numerical experiment for a variety of models. Specifically, we calculated the stationary state probabilities and drew graphs to see the characteristics of the tail behavior. We tested various types of models with various traffic intensities ρ_1 and ρ_2. Among them, for the 8 types of models listed below, we tested systematically with $\rho_1 = .2, .3, \ldots, .9$ and $\rho_2 = .2, .3, \ldots, .9$, and saw the changes of the tail behaviors by the traffic intensities in detail:

$M/E_2/1 \to /E_2/1$, $E_2/E_2/1 \to /E_2/1$, $M/E_2/1 \to /H_2/1$, $E_2/H_2/1 \to /E_2/1$,
$M/H_2/1 \to /E_2/1$, $H_2/E_2/1 \to /E_2/1$, $M/H_2/1 \to /H_2/1$, $E_4/M/1 \to /H_2/1$.

Table 1: Geometric decay of $p(n_1, n_2)$: the case $\rho_2 < \tilde{\rho}_2$

In each model, the upper row represents $g(n_1, n_2)$ for n_1 and n_2 such that $n_2 = (n_1+5)/4, n_1 = 15, 35, \ldots, 95$, and the lower row represents it for n_1 and n_2 such that $n_2 = 4n_1 - 5, n_1 = 5, 10, \ldots, 25$. The traffic intensities ρ_1 and ρ_2 are selected so that $\rho_2 < \tilde{\rho}_2$.

(n_1, n_2)	(5,15) (15,5)	(10,35) (35,10)	(15,55) (55,15)	(20,75) (75,20)	(25,95) (95,25)
$M/E_2/1 \to /E_2/1$	1.4659	1.4725	1.4725	1.4725	1.4725
$\rho_1 = 0.60, \rho_2 = 0.35$	1.4230	1.4682	1.4722	1.4725	1.4725
$M/H_2/1 \to /E_2/1$	0.2773	0.2788	0.2788	0.2788	0.2788
$\rho_1 = 0.60, \rho_2 = 0.40$	0.2798	0.2788	0.2788	0.2788	0.2788
$E_2/E_2/1 \to /E_2/1$	3.0959	3.1120	3.1121	3.1121	3.1121
$\rho_1 = 0.60, \rho_2 = 0.40$	3.1113	3.1122	3.1122	3.1122	3.1122
$H_2/E_2/1 \to /E_2/1$	0.8375	0.8397	0.8397	0.8397	0.8397
$\rho_1 = 0.60, \rho_2 = 0.40$	0.7311	0.8042	0.8289	0.8365	0.8387
$M/E_2/1 \to /H_2/1$	0.7026	0.7026	0.7027	0.7027	0.7027
$\rho_1 = 0.60, \rho_2 = 0.20$	0.6883	0.7018	0.7026	0.7027	0.7027
$M/H_2/1 \to /H_2/1$	0.1538	0.1538	0.1538	0.1538	0.1538
$\rho_1 = 0.60, \rho_2 = 0.40$	0.1570	0.1542	0.1538	0.1538	0.1538
$E_2/H_2/1 \to /E_2/1$	0.4521	0.4557	0.4558	0.4558	0.4558
$\rho_1 = 0.60, \rho_2 = 0.40$	0.4564	0.4558	0.4558	0.4558	0.4558
$E_4/M/1 \to /H_2/1$	0.4924	0.4923	0.4923	0.4923	0.4923
$\rho_1 = 0.60, \rho_2 = 0.40$	0.4991	0.4923	0.4923	0.4923	0.4923

Here, for the two-phase hyperexponential distribution (H_2), we used the one with the density function of the form

$$s(x) = 0.2e^{-4\mu x} + 0.8e^{-\mu x}, \ x > 0.$$

The total number of cases tested exceeds one thousand. For the calculation of the steady-state probabilities, we employed the aggregation/disaggregation method [3, 4]. Since our model has infinite number of states, we have to truncate the state space for both n_1 and n_2 in the calculation. However, in an iteration of the aggregation/disaggregation method, a new value of $x(n_1, n_2; i_0, i_1, i_2)$ is calculated from the current values of neighboring states $x(n_1 - 1, n_2; i_0, i_1, i_2)$, $x(n_1 + 1, n_2 - 1; i_0, i_1, i_2)$ and $x(n_1, n_2 + 1; i_0, i_1, i_2)$. Therefore, if we truncate the state space at $n_1 = \nu_1$ and $n_2 = \nu_2$, we have to estimate the values of $x(\nu_1 + 1, n_2 - 1; i_0, i_1, i_2)$, $1 \le n_2 \le \nu_2$ and $x(n_1, \nu_2 + 1; i_0, i_1, i_2)$, $0 \le n_1 \le \nu_1$. In our experiment, we estimated those values by assuming the geometric decay for these variables, namely, e.g., $x(\nu_1+1, n_2-1; i_0, i_1, i_2)$ was estimated as $\{x(\nu_1, n_2-1; i_0, i_1, i_2)\}^2/x(\nu_1-1, n_2-1; i_0, i_1, i_2)$. Both of the truncation points ν_1 and ν_2 were set to 100 in most of the cases. So the number of states to be calculated was 40,000 for the models listed above with Poisson inputs, and was 80,000 for ones above with other renewal inputs. This number 80,000 is quite large and, by the authors' experiences, it is very near to the limit of the size for the calculation of steady-state probabilities of a Markov chain using today's engineering workstations.

The program was written in C and ran on the SONY NWS-3860 workstation. The computational burden is practically $\mathcal{O}(N)$ with $N = \nu_1 \times \nu_2$, and it increases rapidly as $\rho_k \to 1$. Table 3 tabulates the CPU time for the computation of $E_2/H_2/1 \to /E_2/1$ with $\rho_1 = .6$ and $\rho_2 = .2, .4, .6$ and $.8$.

Table 2: Geometric decay of $p(n_1, n_2)$: the case $\rho_2 > \tilde{\rho}_2$

(a) *faster convergence models*

In each model, the upper row represents $g(n_1, n_2)$ for n_1 and n_2 such that $n_2 = (n_1 + 5)/4, n_1 = 15, 35, \ldots, 95$, and the lower row represents $\overline{g}(n_1, n_2)$ for n_1 and n_2 such that $n_2 = 4n_1 - 5, n_1 = 5, 10, \ldots, 25$. The traffic intensities ρ_1 and ρ_2 are selected so that $\rho_2 > \tilde{\rho}_2$ and $\tilde{a}$ is near to 1.

(n_1, n_2)	(5,15) (15,5)	(10,35) (35,10)	(15,55) (55,15)	(20,75) (75,20)	(25,95) (95,25)
$M/H_2/1 \to /E_2/1$	0.1026	0.1029	0.1022	0.1017	0.1014
$\rho_1 = 0.60, \rho_2 = 0.80$	0.1140	0.1184	0.1193	0.1193	0.1192
$E_2/E_2/1 \to /E_2/1$	0.9333	0.9351	0.9353	0.9353	0.9353
$\rho_1 = 0.60, \rho_2 = 0.70$	0.9141	0.9157	0.9157	0.9156	0.9154
$M/H_2/1 \to /H_2/1$	0.0790	0.0792	0.0789	0.0786	0.0784
$\rho_1 = 0.60, \rho_2 = 0.75$	0.0846	0.0866	0.0869	0.0868	0.0867
$E_2/H_2/1 \to /E_2/1$	0.2162	0.2053	0.2011	0.2002	0.2001
$\rho_1 = 0.60, \rho_2 = 0.85$	0.2776	0.2817	0.2804	0.2801	0.2800
$E_4/M/1 \to /H_2/1$	0.3389	0.3246	0.3235	0.3234	0.3234
$\rho_1 = 0.60, \rho_2 = 0.77$	0.4276	0.4203	0.4192	0.4191	0.4191

(b) *slower convergence models*

This table shows cases in which the convergence is much slower. In each model, the upper row represents $g(n_1, n_2)$ for n_1 and n_2 such that $n_2 = (n_1 + 5)/4, n_1 = 115, 135, \ldots, 195$, and the lower row represents $\overline{g}(n_1, n_2)$ for n_1 and n_2 such that $n_2 = 4n_1 - 5, n_1 = 30, 35, \ldots, 50$. The traffic intensities ρ_1 and ρ_2 are selected so that $\rho_2 > \tilde{\rho}_2$ and $\tilde{a}$ is near to 1.

(n_1, n_2)	(115,30) (30,115)	(135,35) (35,155)	(155,40) (40,155)	(175,45) (45,175)	(195,50) (50,195)
$M/E_2/1 \to /E_2/1$	0.1800	0.1815	0.1829	0.1842	0.1855
$\rho_1 = 0.60, \rho_2 = 0.71$	0.0700	0.0671	0.0647	0.0627	0.0609
$H_2/E_2/1 \to /E_2/1$	0.0957	0.0952	0.0948	0.0947	0.0946
$\rho_1 = 0.60, \rho_2 = 0.70$	0.0206	0.0180	0.0160	0.0142	0.0128
$M/E_2/1 \to /H_2/1$	0.1360	0.1301	0.1294	0.1298	0.1305
$\rho_1 = 0.60, \rho_2 = 0.70$	0.1043	0.1047	0.1050	0.1052	0.1055

Table 3: The CPU time for $E_2/H_2/1 \to /E_2/1$ with $\rho_1 = 0.6$ and $\nu_1 = \nu_2 = 100$

ρ_2	0.2	0.4	0.6	0.8
CPU time [sec.]	16	23	38	158

4. Tail Properties from the Numerical Experiment

The conjecture given in Section 2 is based on a careful observation of the results of the numerical experiments explained in Section 3. Here we show a few results to indicate how the authors reach the conjecture. By the limitation of pages, we take the case of $E_2/H_2/1 \to /E_2/1$ with $\rho_1 = 0.6$ and $\rho_2 = 0.8$ as a typical example, and show its tail properties in detail. We start with observing the ratio of two neighboring joint probabilities of numbers of customers in the steady state.

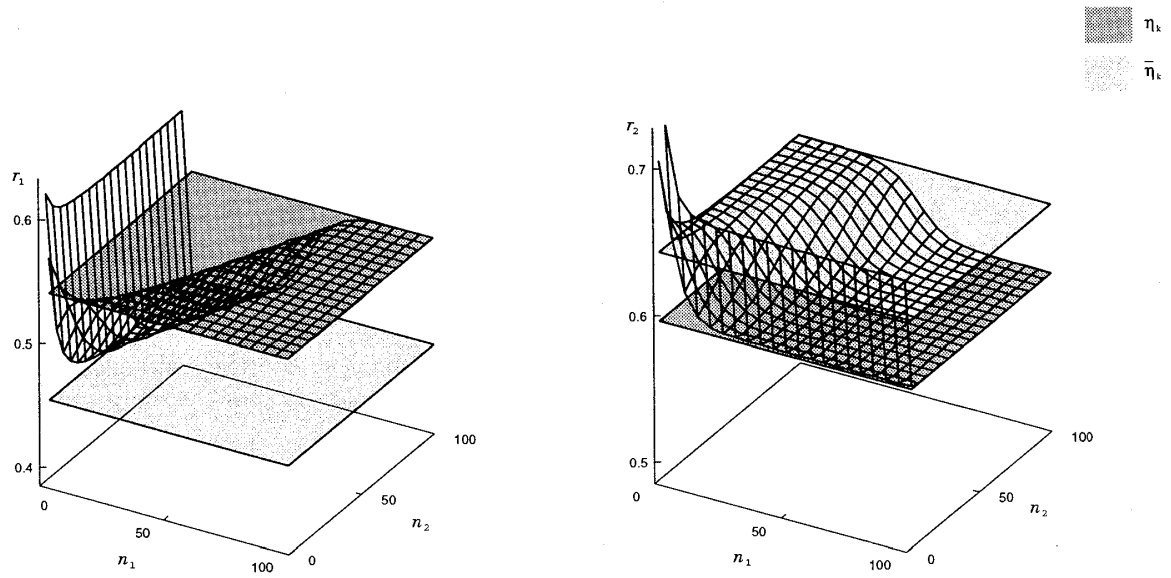

a: $r_1(n_1, n_2) = \frac{p(n_1+1,n_2)}{p(n_1,n_2)}$ b: $r_2(n_1, n_2) = \frac{p(n_1,n_2+1)}{p(n_1,n_2)}$

Figure 2: r_k behavior in $E_2/H_2/1 \to /E_2/1$ $(\rho_1 = 0.6, \rho_2 = 0.8)$

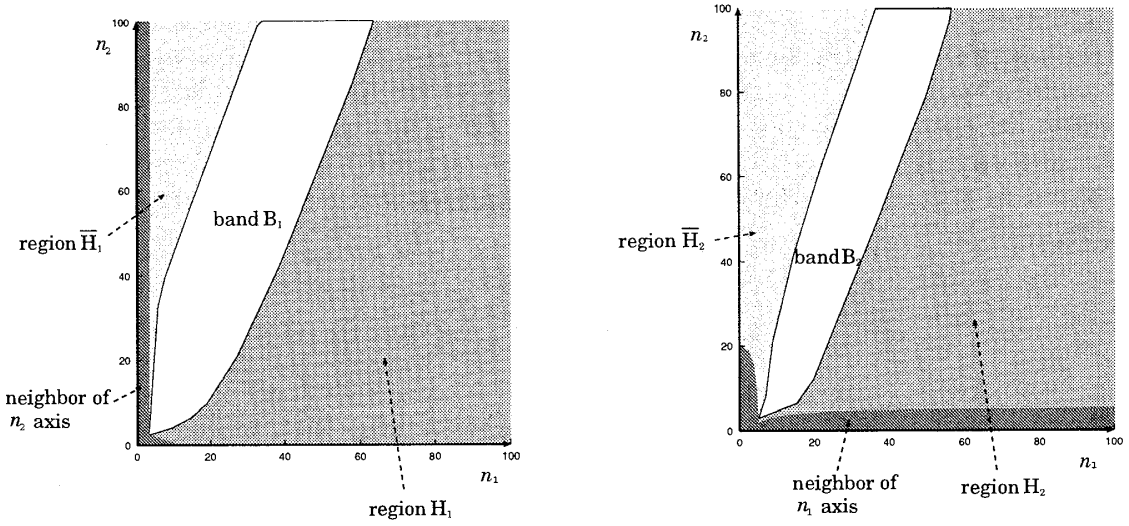

a: r_1 b: r_2

Figure 3: Characterization of r_k surface

4.1. Decay Rates of the Joint Queue-lengths Probability

Let $p(n_1, n_2)$ be the joint probability that there exist n_k customers in the kth stage $(k = 1, 2)$ in the steady state. Namely, $p(n_1, n_2) = \sum_{i_0} \sum_{i_1} \sum_{i_2} x(n_1, n_2; i_0, i_1, i_2)$. We are interested in the ratios of neighboring $p(n_1, n_2)$'s:

$$r_1(n_1, n_2) = \frac{p(n_1 + 1, n_2)}{p(n_1, n_2)} \quad \text{and} \quad r_2(n_1, n_2) = \frac{p(n_1, n_2 + 1)}{p(n_1, n_2)}.$$

Figures 2a and 2b show graphs of $r_1(n_1, n_2)$ and $r_2(n_1, n_2)$. In each figure, the graph of $r_k(n_1, n_2)$ is a curved surface represented by a lattice. A dark gray plane indicates a constant η_k $(\eta_1 = 0.543, \eta_2 = 0.593)$ and a light gray plane indicates another constant

$\overline{\eta}_k$ ($\overline{\eta}_1 = 0.457, \overline{\eta}_2 = 0.640$). Both of these constants are given as solutions of systems of equations which will be presented in Section 5.

In Figure 2a, we see that $r_1(n_1, n_2)$ is relatively large very near the n_2 axis but it is in between η_1 and $\overline{\eta}_1$ in most of the region of (n_1, n_2). Especially $r_1(n_1, n_2)$ is close to η_1 in a region in which n_1 is relatively larger than n_2 and it is close to $\overline{\eta}_1$ in a region in which n_2 is relatively larger than n_1 though the latter might not be seen clearly from the figure.

Figure 3a shows regions of (n_1, n_2) in which $r_1(n_1, n_2)$ is close to η_1 or $\overline{\eta}_1$. In the dark gray region, labeled H_1, $r_1(n_1, n_2)$ is close to η_1, namely $|r_1(n_1, n_2) - \eta_1| < \varepsilon_1$ with $\varepsilon_1 = 0.1 \times |\eta_1 - \overline{\eta}_1|$, and in the light gray region, labeled $\overline{\mathrm{H}}_1$, $r_1(n_1, n_2)$ is close to $\overline{\eta}_1$, namely $|r_1(n_1, n_2) - \overline{\eta}_1| < \varepsilon_1$. (Here we take the particular value of ε_1 for the convenience of the explanation. We may take a smaller value if we need more accuracy in the subsequent approximations.) The band B_1 between H_1 and $\overline{\mathrm{H}}_1$ represents the region where $r_1(n_1, n_2)$ smoothly changes from $\eta_1 - \varepsilon_1$ to $\overline{\eta}_1 + \varepsilon_1$. We note that the region H_1 covers the n_1 axis while $\overline{\mathrm{H}}_2$ does not n_2 axis.

Similarly, in Figure 2b, we see that $r_2(n_1, n_2)$ is relatively large very near the n_1 axis but it is in between η_2 and $\overline{\eta}_2$ in most of the region of (n_1, n_2). Especially $r_2(n_1, n_2)$ is close to η_2 in a region in which n_1 is relatively larger than n_2 and it is close to $\overline{\eta}_2$ in a region in which n_2 is relatively larger than n_1.

Figure 3b shows a decomposition of the n_1-n_2 plane by $r_2(n_1, n_2)$. The ratio $r_2(n_1, n_2)$ is close to η_2 in the dark gray region H_2, and is close to $\overline{\eta}_2$ in the light gray region $\overline{\mathrm{H}}_2$. The band B_2 represents the region where $r_2(n_1, n_2)$ smoothly changes from $\eta_2 - \varepsilon_2$ to $\overline{\eta}_2 + \varepsilon_2$ where $\varepsilon_2 = 0.1 \times |\eta_2 - \overline{\eta}_2|$. In this case n_2-axis is included in $\overline{\mathrm{H}}_2$, but n_1-axis is not in H_2.

Figures 3a resembles 3b in some sense. H_1 mostly coincides with H_2, and $\overline{\mathrm{H}}_1$ does with $\overline{\mathrm{H}}_2$. Hence, $r_1(n_1, n_2) \approx \eta_1$ and $r_2(n_1, n_2) \approx \eta_2$ in the region $\mathrm{H}_1 \bigcap \mathrm{H}_2$, and $r_1(n_1, n_2) \approx \overline{\eta}_1$ and $r_2(n_1, n_2) \approx \overline{\eta}_2$ in the region $\overline{\mathrm{H}}_1 \bigcap \overline{\mathrm{H}}_2$, where "$\approx$" indicates that both sides are approximately equal. Hence

$$\frac{p(n_1 + l_1, n_2 + l_2)}{p(n_1, n_2)} \approx \begin{cases} \eta_1^{l_1} \eta_2^{l_2}, & \text{if } (n_1, n_2),\ (n_1 + l_1, n_2 + l_2) \in \mathrm{H}_1 \bigcap \mathrm{H}_2, \\ \overline{\eta}_1^{l_1} \overline{\eta}_2^{l_2}, & \text{if } (n_1, n_2),\ (n_1 + l_1, n_2 + l_2) \in \overline{\mathrm{H}}_1 \bigcap \overline{\mathrm{H}}_2. \end{cases} \tag{4.1}$$

The band B_2 lies almost on the same position as B_1, though the band width is a bit narrower. In these graphs, the bands B_1 and B_2 seem to keep their widths constant. More definitely, they are included in a region $\{(n_1, n_2) : \tilde{a} n_1 + \underline{b} < n_2 < \tilde{a} n_1 + \overline{b}\}$ bounded by two parallel lines with a common slope $\tilde{a} = 2.28$ and segments $\underline{b} = -48$ and $\overline{b} = 26$ as shown in Figure 4. The value $\tilde{a}$ of the slope will be discussed in Section 4.4 and in Section 5.

4.2. Geometric Form of the Joint Queue-length Probability

It seems that $p(n_1, n_2)$ is written approximately in a geometric form in the n_1-n_2 plane:

$$p(n_1, n_2) \approx \begin{cases} G\, \eta_1^{n_1} \eta_2^{n_2}, & \text{if } (n_1, n_2) \in \mathrm{H}_1 \bigcap \mathrm{H}_2, \\ \overline{G}\, \overline{\eta}_1^{n_1} \overline{\eta}_2^{n_2}, & \text{if } (n_1, n_2) \in \overline{\mathrm{H}}_1 \bigcap \overline{\mathrm{H}}_2, \end{cases} \tag{4.2}$$

where G and $\overline{G}$ are certain constants independent of n_1 and n_2.

To justify this from numerical results, we draw graphs of the ratios $g(n_1, n_2)$ and $\overline{g}(n_1, n_2)$ defined in Section 2.2. Figure 5a shows that $g(n_1, n_2)$ almost coincides with a constant $G = 5.67 \times 10^{-3}$ when $(n_1, n_2) \in \mathrm{H}_1 \bigcap \mathrm{H}_2$, and Figure 5b shows that $\overline{g}(n_1, n_2)$ mostly coincides with a constant $\overline{G} = 1.51 \times 10^{-2}$ ($\neq G$) when $(n_1, n_2) \in \overline{\mathrm{H}}_1 \bigcap \overline{\mathrm{H}}_2$. Note that, in these graphs, we cut the region where $n_1 < 5$ or $n_2 < 5$ to make the graphs easier to see the behavior when n_1 and n_2 are large. Hereafter we will use this convention in all graphs except Figure 9.

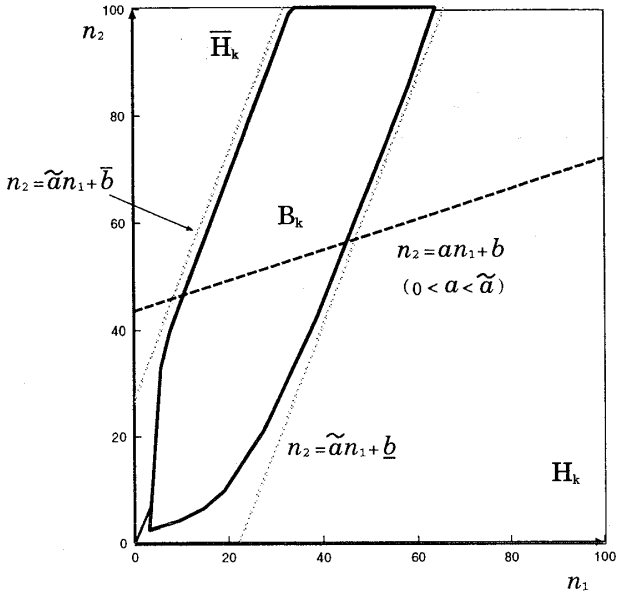

Figure 4: constraint lines for band B_k

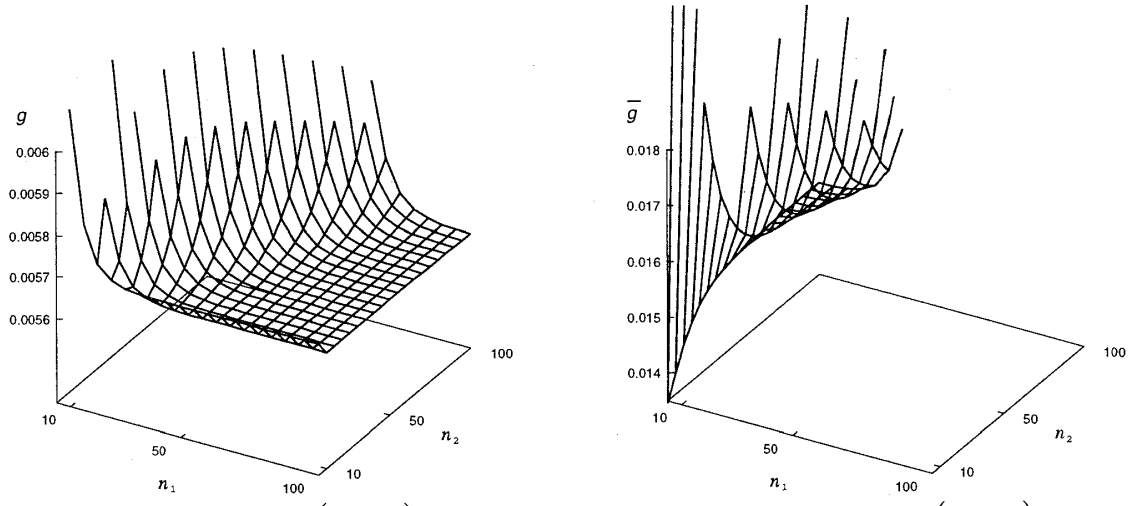

a: $g(n_1,n_2)=\dfrac{p(n_1,n_2)}{\eta_1^{n_1}\eta_2^{n_2}}$ b: $\overline{g}(n_1,n_2)=\dfrac{p(n_1,n_2)}{\overline{\eta}_1^{n_1}\overline{\eta}_2^{n_2}}$

Figure 5: Behaviors of $g(n_1,n_2)$ and $\overline{g}(n_1,n_2)$ in $E_2/H_2/1 \to /E_2/1$ with $\rho_1=0.6, \rho_2=0.8$

4.3. Approximate Independence of Phases

The individual state probabilities $x(n_1,n_2;i_0,i_1,i_2)$ satisfy similar properties to those of $p(n_1,n_2)$ above. Hence it is expected that the conditional probability of phases

$$y(i_0,i_1,i_2|n_1,n_2)=\frac{x(n_1,n_2;i_0,i_1,i_2)}{p(n_1,n_2)}$$

almost coincides with a constant in $\mathrm{H}_1 \bigcap \mathrm{H}_2$, and with another constant in $\overline{\mathrm{H}}_1 \bigcap \overline{\mathrm{H}}_2$. In fact, Figure 6 shows that $y(1,1,1|n_1,n_2)$ behaves like $r_k(n_1,n_2)$. That is, $y(i_0,i_1,i_2|n_1,n_2)$ coincides with a constant $c(i_0,i_1,i_2)$ in $\mathrm{H}_1 \bigcap \mathrm{H}_2$, and with the other constant $\overline{c}(i_0,i_1,i_2)$ in $\overline{\mathrm{H}}_1 \bigcap \overline{\mathrm{H}}_2$. Furthermore, we can see that both $c(i_0,i_1,i_2)$ and $\overline{c}(i_0,i_1,i_2)$ are decomposed into

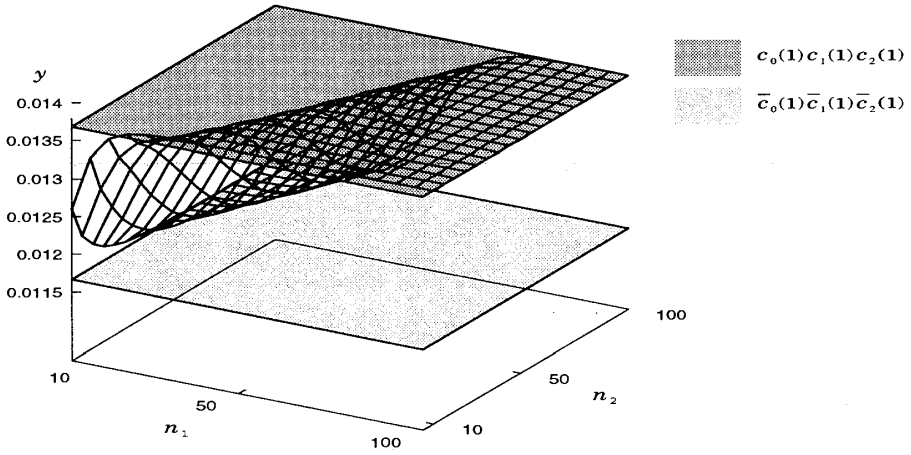

Figure 6: Behavior of $y(1,1,1|n_1,n_2)$ in $E_2/H_2/1 \to /E_2/1$ with $\rho_1 = 0.6, \rho_2 = 0.8$

three components:

$$y(i_0,i_1,i_2|n_1,n_2) \approx \begin{cases} c_0(i_0)c_1(i_1)c_2(i_2) & \text{if } (n_1,n_2) \in \mathrm{H}_1 \cap \mathrm{H}_2, \\ \bar{c}_0(i_0)\bar{c}_1(i_1)\bar{c}_2(i_2) & \text{if } (n_1,n_2) \in \overline{\mathrm{H}}_1 \cap \overline{\mathrm{H}}_2. \end{cases} \tag{4.3}$$

Here $c_0(i_0)$ or $\bar{c}_0(i_0)$ can be regarded as the asymptotic conditional probability of the phase i_0 of the arrival process, and $c_k(i_k)$ or $\bar{c}_k(i_k)$ $(k = 1, 2)$ as the asymptotic conditional probability of the phase i_k of the service process at the kth stage. This property can be validated by the numerical results of $y(i_0, i_1, i_2 \mid n_1, n_2)$ together with the values of $c_k(i_k)$'s and $\bar{c}_k(i_k)$'s given by (5.8) in Section 5. The value of them for $E_2/H_2/1 \to /E_2/1$ are listed in Tables 4 and 5. It is shown that $y(i_0, i_1, i_2 \mid 90, 10)$ almost coincides with $c_0(i_0)c_1(i_1)c_2(i_2)$, and that $y(i_0, i_1, i_2 \mid 10, 90)$ almost coincides with $\bar{c}_0(i_0)\bar{c}_1(i_1)\bar{c}_2(i_2)$ for all combinations of (i_0, i_1, i_2). Note that $(90, 10) \in \mathrm{H}_1 \cap \mathrm{H}_2$ while $(10, 90) \in \overline{\mathrm{H}}_1 \cap \overline{\mathrm{H}}_2$.

Table 4: $c_k(i_k)$ and $\bar{c}_k(i_k)$ in $E_2/H_2/1 \to /E_2/1$ with $\rho_1 = 0.6$, $\rho_2 = 0.8$

i_k	$c_0(i_0)$	$c_1(i_1)$	$c_2(i_2)$	$\bar{c}_0(i_0)$	$\bar{c}_1(i_1)$	$\bar{c}_2(i_2)$
1	0.0576	0.0546	0.4351	0.5967	0.0440	0.4444
2	0.4243	0.9454	0.5649	0.4033	0.9560	0.5556

4.4. Variation of Regions and Bands

Now we shall see how the regions H_k, $\overline{\mathrm{H}}_k$ and the band B_k vary according to the traffic intensities ρ_1 and ρ_2.

Figure 7 shows the graphs of $r_1(n_1, n_2)$ for the model $E_2/H_2/1 \to /E_2/1$ with fixed $\rho_1 = 0.6$ and varying $\rho_2 = 0.4 \sim 0.9$. When ρ_2 is small, $\overline{\eta}_1$ is far below η_1 and $r_1(n_1, n_2)$ coincides with η_1 almost on the whole n_1-n_2 plane. This means that H_1 covers the whole n_1-n_2 plane. The larger ρ_2 becomes, the closer $\overline{\eta}_1$ comes to η_1, and when $\rho_2 = 0.8$ the region $\overline{\mathrm{H}}_1$ appears. $\overline{\mathrm{H}}_1$ becomes larger than H_1 when $\rho_2 = 0.9$.

Figure 8 shows the corresponding graphs of $r_2(n_1, n_2)$. In these graphs we also see that $\overline{\mathrm{H}}_2$ appears only when $\rho_2 = 0.8$ and 0.9. Now we shall see the movement of the planes η_2 and $\overline{\eta}_2$. When ρ_2 is small, the plane $\overline{\eta}_2$ is far below the plane η_2. As ρ_2 becomes larger the plane $\overline{\eta}_2$ becomes closer to the plane η_2, but still below the plane η_2 for $\rho_2 \leq 0.7$. When ρ_2

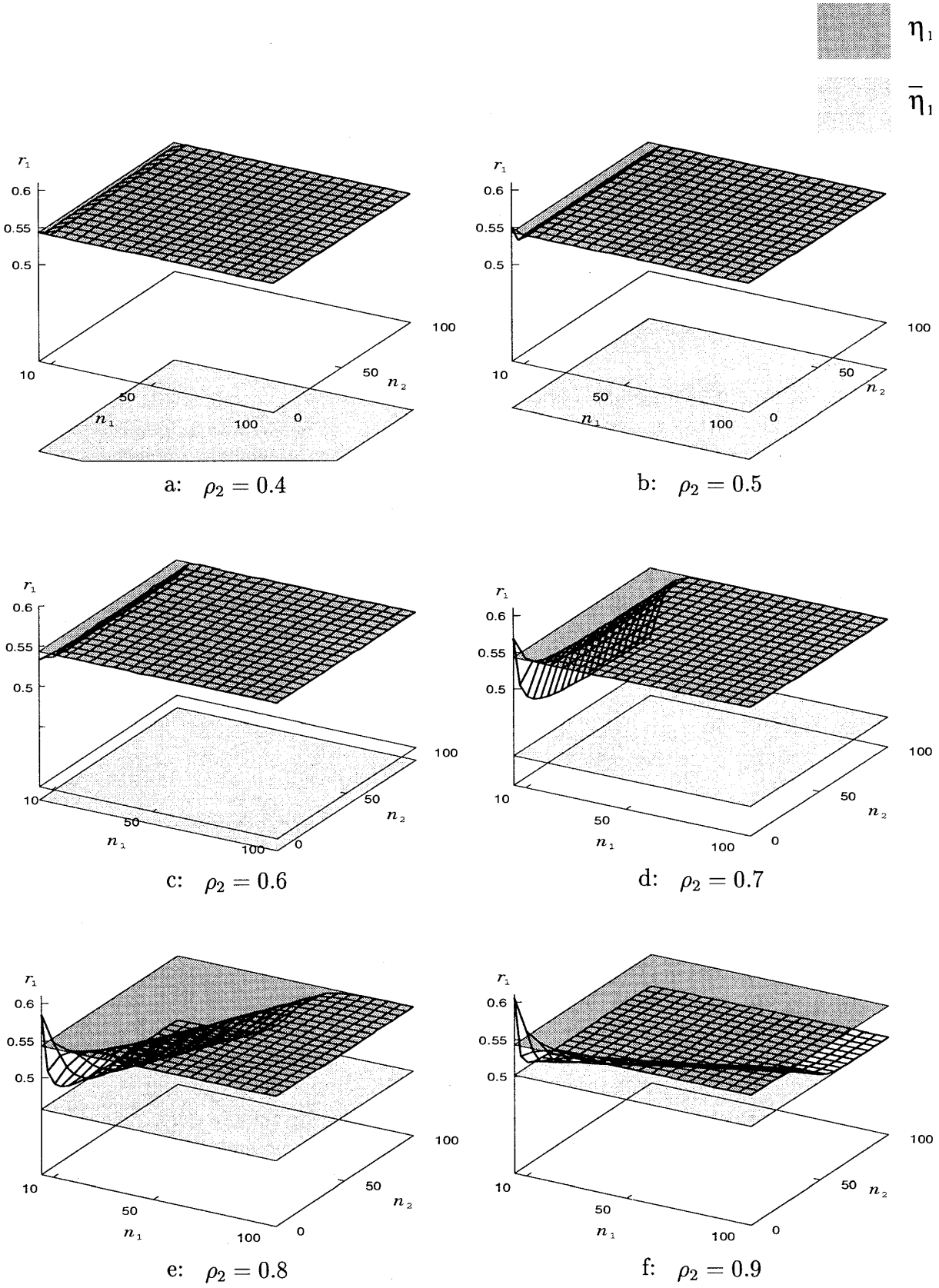

Figure 7: r_1 behavior in $E_2/H_2/1 \rightarrow /E_2/1$ $(\rho_1 = 0.6)$

Table 5: $c_k(i_k)$ and $\overline{c}_k(i_k)$ in $E_2/H_2/1 \to /E_2/1$ with $\rho_1 = 0.6$, $\rho_2 = 0.8$

(i_0, i_1, i_2)	$c_0(i_0)c_1(i_1)c_2(i_2)$	$y(i_0, i_1, i_2 \mid 90, 10)$	$\overline{c}_0(i_0)\overline{c}_1(i_1)\overline{c}_2(i_2)$	$y(i_0, i_1, i_2 \mid 10, 90)$
$(1,1,1)$	1.368×10^{-2}	1.368×10^{-2}	1.166×10^{-2}	1.166×10^{-2}
$(1,1,2)$	1.776×10^{-2}	1.776×10^{-2}	1.457×10^{-2}	1.458×10^{-2}
$(1,2,1)$	2.368×10^{-1}	2.368×10^{-1}	2.535×10^{-1}	2.535×10^{-1}
$(1,2,2)$	3.074×10^{-1}	3.074×10^{-1}	3.169×10^{-1}	3.169×10^{-1}
$(2,1,1)$	1.008×10^{-2}	1.008×10^{-2}	7.882×10^{-3}	7.886×10^{-3}
$(2,1,2)$	1.309×10^{-2}	1.309×10^{-2}	9.853×10^{-3}	9.858×10^{-3}
$(2,2,1)$	1.745×10^{-1}	1.745×10^{-1}	1.714×10^{-1}	1.714×10^{-1}
$(2,2,2)$	2.266×10^{-1}	2.266×10^{-1}	2.142×10^{-1}	2.142×10^{-1}

becomes to 0.8, the plane $\overline{\eta}_2$ comes above the plane η_2, and at the same time the region $\overline{\mathrm{H}}_2$ appears. If we denote by $\tilde{\rho}_2$ the value of ρ_2 at which $\eta_2 = \overline{\eta}_2$, this seems to indicate that the region $\overline{\mathrm{H}}_2$ disappears when ρ_2 is less than $\tilde{\rho}_2$ and $\overline{\mathrm{H}}_2$ appears when ρ_2 exceeds $\tilde{\rho}_2$.

$\overline{\mathrm{H}}_1$ seems to appear at the same time as $\overline{\mathrm{H}}_2$. We will see this more in detail. Figure 9 shows the movement of the bands B_1 and B_2. The bands bounded by thin lines indicate B_1 for $\rho_2 = 0.75 \sim 0.90$, and those bounded by bold lines indicate B_2.

It is likely that these behaviors of the bands are related with those of η_k and $\overline{\eta}_k$. In Figure 5, both $g(n_1, n_2)$ and $\overline{g}(n_1, n_2)$ diverge to $+\infty$ when they are outside of $\mathrm{H}_1 \cap \mathrm{H}_2$ or $\overline{\mathrm{H}}_1 \cap \overline{\mathrm{H}}_2$. This indicates that $\eta_1^{n_1}\eta_2^{n_2}$ is greater than $\overline{\eta}_1^{n_1}\overline{\eta}_2^{n_2}$ in the region $\mathrm{H}_1 \cap \mathrm{H}_2$, and that $\overline{\eta}_1^{n_1}\overline{\eta}_2^{n_2}$ is greater than $\eta_1^{n_1}\eta_2^{n_2}$ in the region $\overline{\mathrm{H}}_1 \cap \overline{\mathrm{H}}_2$.

Hence we can guess that the bands B_1 and B_2 lie on the line determined by $\eta_1^{n_1}\eta_2^{n_2} = \overline{\eta}_1^{n_1}\overline{\eta}_2^{n_2}$, or equivalently,

$$n_2 = \tilde{a} n_1 \quad \text{with } \tilde{a} = -\frac{\log \overline{\eta}_1/\eta_1}{\log \overline{\eta}_2/\eta_2}. \tag{4.4}$$

Each broken line in Figure 9 indicates this line for $\rho_2 = 0.75 \sim 0.90$. One can see that the line moves almost together with the bands.

5. Equations for η_k, $\overline{\eta}_k$ and $\tilde{\rho}_2$

The properties discussed in the previous section are for the specific model $E_2/H_2/1 \to /E_2/1$. We can see similar properties in most of cases.

To the authors' knowledge, there are no papers which investigate such tail properties theoretically. However, through the study, they have a strong confidence that the values of η_k and $\overline{\eta}_k$ $(k = 1, 2)$ are given as solutions of some simultaneous equations written with LSTs of interarrival and service time distributions. In this section we present the equations and summarize some basic properties of η_k and $\overline{\eta}_k$. The assumptions to derive the equations and a brief explanation of the derivation process are given at the end of this section.

Let $T^*(s)$ be the LST of the interarrival time distribution $PH(\boldsymbol{\alpha}, \boldsymbol{T})$. Denoting by $-\tau < 0$ an abscissa of convergence of T^*, the function $T^*(s)$ is then defined, positive and convex decreasing on the interval $(-\tau, \infty)$ [1]. Similarly, we denote by $S_k^*(s)$ the LST of the service time distribution $PH(\boldsymbol{\beta}, \boldsymbol{S}_k)$ for the k-th stage, and by $-\sigma_k < 0$ an abscissa of convergence of S_k^*. Then $S_k^*(s)$ is defined, positive and convex decreasing on the interval $(-\sigma_k, \infty)$. When we mention about roots of an equation, we refer only real roots in the domain of the equation and count the number of roots by taking the multiplicity into account. For example, every double root is counted twice.

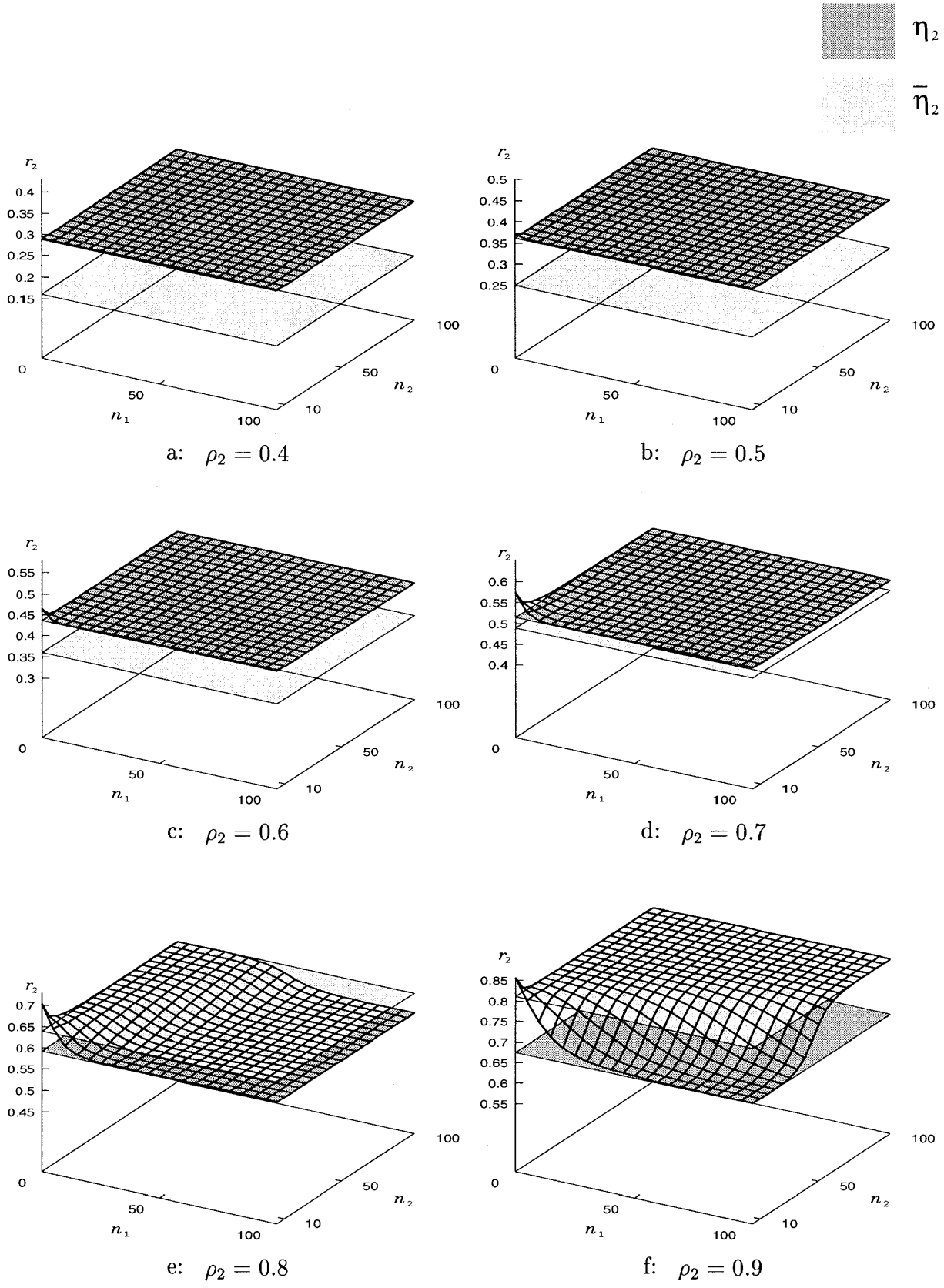

Figure 8: r_2 behavior in $E_2/H_2/1 \rightarrow /E_2/1$ $(\rho_1 = 0.6)$

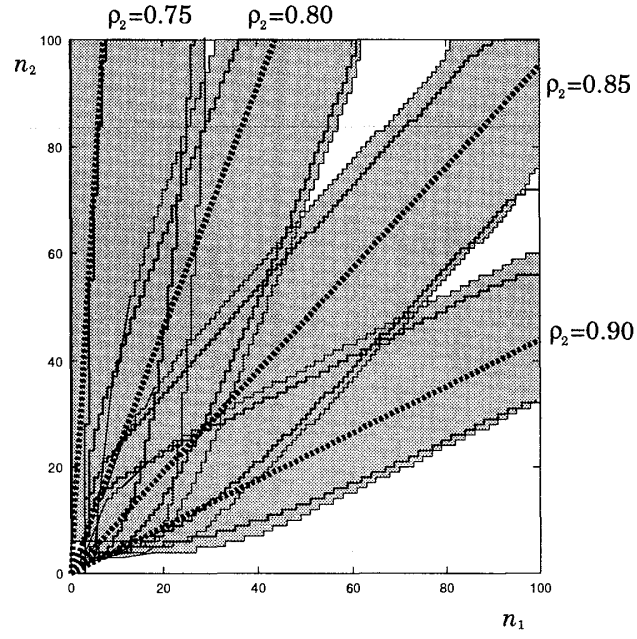

Figure 9: Movement of B_1 and B_2 in $E_2/H_2/1 \to /E_2/1$ with $\rho_1 = 0.6$

Consider the simultaneous equations

$$\left\{\begin{array}{rcl} T^*(s_0)S_1^*(-s_0) & = & 1, \\ T^*(s_0)S_1^*(s_1)S_2^*(s_2) & = & 1, \\ s_0 + s_1 + s_2 & = & 0. \end{array}\right. \tag{5.1}$$

Let $f(s_0) = T^*(s_0)S_1^*(-s_0)$. Then $f(s_0)$ is a convex function of s_0 on $(-\tau, \sigma_1)$, and $f(0) = 1$. Hence the equation $f(s_0) = 1$ has two roots one of which is $s_0 = 0$. The derivative of $f(s_0)$ at $s_0 = 0$ is negative since $f'(0) = T^{*\prime}(0) - S_1^{*\prime}(0) = -1/\lambda + 1/\mu_1 = -(1-\rho_1)/\lambda < 0$. Hence the other root $s_0 = \omega_0$ is positive.

For the second equation of (5.1), eliminating s_1 by the third equation and inserting $s_0 = \omega_0$, we have

$$g(s_2) = T^*(\omega_0)S_1^*(-\omega_0 - s_2)S_2^*(s_2) = 1. \tag{5.2}$$

$g(s_2)$ is a convex function of s_2 on $(-\sigma_2, \sigma_1 - \omega_0)$. The equation (5.2) has a trivial root $s_2 = 0$, and hence it has one more root $s_2 = \omega_2$. We set $\omega_1 = -\omega_0 - \omega_2$. This triplet $(\omega_0, \omega_1, \omega_2)$ is our desired solution of (5.1), and we let

$$\eta_1 = T^*(\omega_0), \quad \eta_2 = \frac{1}{S_2^*(\omega_2)}. \tag{5.3}$$

Since ω_0 is positive, η_1 is strictly less than 1. Furthermore, η_1 is a monotone increasing function of ρ_1, and $\eta_1 \downarrow 0$ as $\rho_1 \downarrow 0$ while $\eta_1 \uparrow 1$ as $\rho_1 \uparrow 1$. On the other hand, ω_2 is negative if ρ_2 is small but it may be positive if ρ_2 becomes large, and hence η_2 may exceed 1. η_2 can be regarded as a function of both ρ_1 and ρ_2. As a function of ρ_2, η_2 is monotone increasing and $\eta_2 \downarrow 0$ as $\rho_2 \downarrow 0$.

For $\overline{\eta}_k$'s, consider the simultaneous equations

$$\left\{\begin{array}{rcl} T^*(-\overline{s}_2)S_2^*(\overline{s}_2) & = & 1, \\ T^*(\overline{s}_0)S_1^*(\overline{s}_1)S_2^*(\overline{s}_2) & = & 1, \\ \overline{s}_0 + \overline{s}_1 + \overline{s}_2 & = & 0. \end{array}\right. \tag{5.4}$$

A similar argument for the equations (5.1) can be applied to (5.4). The first equation defined on $(-\sigma_2, \tau)$ has two roots, zero and $\overline{\omega}_2$. Since $\rho_2 < 1$, $\overline{\omega}_2$ is strictly negative. By inserting $\overline{s}_2 = \overline{\omega}_2$ and $\overline{s}_1 = -\overline{s}_0 - \overline{\omega}_2$ into the left hand side of the second equation, we have an equation for $\overline{s}_2 = \overline{\omega}_2$. The left hand side of this equation is a convex function, and hence the equation has two roots. One is a trivial root $\overline{s}_0 = -\overline{\omega}_2$, and we denote the other as $\overline{\omega}_0$. We set $\overline{\omega}_1 = -\overline{\omega}_0 - \overline{\omega}_2$. This triplet $(\overline{\omega}_0, \overline{\omega}_1, \overline{\omega}_2)$ is the desired solution of (5.4). For this triplet, we set

$$\overline{\eta}_2 = \frac{1}{S_2^*(\overline{\omega}_2)}, \quad \overline{\eta}_1 = T^*(\overline{\omega}_0). \tag{5.5}$$

Since $\overline{\omega}_2$ is negative, $\overline{\eta}_2$ is less than 1. Moreover, $\overline{\eta}_2$ is a monotone increasing function of ρ_2, and $\overline{\eta}_2 \downarrow 0$ as $\rho_2 \downarrow 0$ while $\overline{\eta}_2 \uparrow 1$ as $\rho_2 \uparrow 1$. $\overline{\omega}_0$ may take positive or negative value, and hence $\overline{\eta}_1$ may be greater than 1. $\overline{\eta}_1$ is a function of both ρ_1 and ρ_2, and $\overline{\eta}_1 \to \eta_1$ as $\rho_1 \uparrow 1$.

Using η_k and $\overline{\eta}_k$ above, the slope $\tilde{a}$ of bands B_k is given by (4.4) in most of the models. In Section 4.4, we defined $\tilde{\rho}_2$ as ρ_2 at which $\eta_2 = \overline{\eta}_2$. However, this definition is not suitable in a general situation since such $\tilde{\rho}_2$ may not be unique. We can show that, for fixed ρ_1, there exists a unique ρ_2 such that

$$\eta_1 = \eta_2 = \overline{\eta}_2. \tag{5.6}$$

This ρ_2 is suitable for $\tilde{\rho}_2$. When $\tilde{a}$ is well-defined for all $\rho_2 \in (0,1)$ except for the point $\rho_2 = \tilde{\rho}_2$, $\tilde{a}$ is strictly negative for $\rho_2 < \tilde{\rho}_2$ and is strictly positive for $\rho_2 > \tilde{\rho}_2$. Further, usually $\tilde{a} \uparrow +\infty$ as $\rho_2 \downarrow \tilde{\rho}_2$, and $\tilde{a} \downarrow 0$ as $\rho_2 \uparrow 1$.

Note that $\tilde{a}$ in (4.4) cannot be defined for $E_j/E_j/1 \to /E_j/1$ with $j = 1, 2, \ldots$, in which $\eta_1 = \overline{\eta}_1 = \rho_1^j$ and $\eta_2 = \overline{\eta}_2 = \rho_2^j$. In this case, a perturbation analysis indicates that

$$\tilde{\rho}_2 = \rho_2 \quad \text{and} \quad \tilde{a} = \frac{1-\rho_2}{\rho_1 - \rho_2} \tag{5.7}$$

are plausible definitions for these models.

For $c_k(i_k)$, we have the following expressions. Let $\boldsymbol{c}_k$ be the stochastic vector whose i_k-th element is $c_k(i_k)$.

$$\begin{aligned} \boldsymbol{c}_0 &= \frac{\omega_0}{1-\eta_1}\boldsymbol{\alpha}(\omega_0 \boldsymbol{I} - \boldsymbol{T})^{-1}, \\ \boldsymbol{c}_1 &= \frac{\omega_1}{1-\eta_2/\eta_1}\boldsymbol{\beta}_1(\omega_1 \boldsymbol{I} - \boldsymbol{S}_1)^{-1}, \\ \boldsymbol{c}_2 &= \frac{\omega_2}{1-1/\eta_2}\boldsymbol{\beta}_2(\omega_2 \boldsymbol{I} - \boldsymbol{S}_2)^{-1}. \end{aligned} \tag{5.8}$$

For $\overline{c}_k(i_k)$, we have similar expressions with $\overline{\omega}_k$ and $\overline{\eta}_k$ in places of ω_k and η_k, respectively.

The derivation process of the equations in (5.1) and (5.4) is rather complicated. Here we give basic assumptions for the equations and briefly outline the derivation process. The complete derivation process and related discussions will be given in a separate paper.

For (5.1), we assume a geometric decay property for large n_1: There exists a constant η_1 such that

$$x(n_1, n_2; i_0, i_1, i_2) = \eta_1 x(n_1 - 1, n_2; i_0, i_1, i_2) \quad \text{for } \forall i_0, i_1, i_2 \text{ and } n_2 = 0, 1, 2, \ldots. \tag{5.9}$$

For fixed n_1 we consider the balance equation around the state $(n_1, n_2; i_0, i_1, i_2)$. We can use (5.9) to eliminate $x(n_1 - 1, *; *, *, *)$'s and $x(n_1 + 1, *; *, *, *)$'s in the equation so that

the equation contains only $x(n_1, *; *, *, *)$'s. By considering such balance equations for all i_0, i_1, i_2 and $n_2 = 0, 1, 2, \ldots$, we can show that $x(n_1, n_2; i_0, i_1, i_2)$ takes a matrix-geometric form. If we use a similar technique to the one in [5], we obtain the relations in (5.1), (5.3) and (5.8). Thus, roughly speaking, if the steady-state distribution has geometric tail in the direction of n_1-axis, the decay parameters are given by (5.3).

On the other hand, to derive the second and the third equations in (5.4) we assume for large n_2 that there exists a constant $\overline{\eta}_2$ such that

$$x(n_1, n_2; i_0, i_1, i_2) = \overline{\eta}_2 x(n_1, n_2 - 1; i_0, i_1, i_2) \quad \text{for } \forall i_0, i_1, i_2 \text{ and } n_1 = 0, 1, 2, \ldots.$$

Furthermore, to derive the first equation in (5.4), we have to assume that $x(n_1, n_2; i_0, i_1, i_2)$ is of the form $x_1(n_1; i_0, i_1)x_2(n_2, i_2)$. A similar process to the one above leads us to the relations in (5.4), (5.5) and $\overline{c}_k$ version of (5.8). In case of (5.1), the assumption of asymptotic product form is not necessary because instead we can use the fact that the behavior of the first stage is never affected by the second stage.

Thus, the above equations for the characteristic constants of the tail probabilities are derived from geometric decay assumptions and some product form assumptions. However, the multiplicative constants G and $\overline{G}$ cannot be obtained in this line of derivation. To get the values of them, we have to execute some simulations or to solve the balance equations numerically. In the latter case, if we use the geometric decay property above, we can get the values of them with much smaller computational burden.

Acknowledgments

The authors express their sincere thanks to Professor Naoki Makimoto for giving them valuable comments through intensive discussions. They also thank anonymous referees for their helpful suggestions on the revision of the manuscript.

References

[1] Marcel F. Neuts. The abscissa of convergence of the Laplace-Stieltjes transform of a PH-distribution. *Communications in Statistics. Simulation and Computation*, **13**: pp.367–373, 1984.

[2] Marcel F. Neuts and Yukio Takahashi. Asymptotic behavior of the stationary distributions in the GI/PH/c queue with heterogeneous servers. *Z. Wahrscheinlichkeitstheorie verw. Gebiete*, **57**: pp.441–452, 1981.

[3] Paul J. Schweitzer. Aggregation methods for large Markov chains. In G. Iazeolla, P. J. Courtois, and A. Hordijk, editors, *Mathematical Computer Performance and Reliability*, pages pp.275–286. North-Holland, Amsterdam, 1984.

[4] Yukio Takahashi. A lumping method for numerical calculations of stationary distributions of Markov chains. Research Reports on Information Sciences B-18, Tokyo Institute of Technology, June 1975.

[5] Yukio Takahashi. Asymptotic exponentiality of the tail of the waiting time distribution in a PH/PH/c queue. *Advances in Applied Probability*, **13**: pp.619–630, 1981.

Kou FUJIMOTO: fujimoto@is.titech.ac.jp
Yukio TAKAHASHI: yukio@is.titech.ac.jp
Department of Mathematical and Computing Sciences
Tokyo Institute of Technology
Ookayama, Meguro-ku, Tokyo 152 Japan